A Mechanistic Growth Model for Inorganic Crystals: Solid-State Interactions

Preshit Dandekar and Michael F. Doherty
Dept. of Chemical Engineering, University of California Santa Barbara, Santa Barbara, CA 93106-5080

DOI 10.1002/aic.14597
Published online September 16, 2014 in Wiley Online Library (wileyonlinelibrary.com)

Growth shapes of inorganic crystalline solids govern material properties such as catalytic activity and selectivity, solar cell efficiency, and so forth. A systematic understanding of the crystal growth process and the solid-state interactions within inorganic crystals should help to engineer crystal shapes. A general model that identifies periodic bond chains in inorganic crystals while accounting for the long-range electrostatic interactions is presented. The variation in the electronic structure and the partial charges of growth units on the inorganic crystal surfaces has been captured using the bond valence model. The electrostatic interaction energies in the kink sites of inorganic crystals were calculated using a space partitioning method that is computationally efficient. This model provides a quantitative explanation for the asymmetric growth spirals formed on the $(10\bar{1}4)$ surface of calcite. This methodology for studying solid-state interactions can be used with a mechanistic growth model to predict the morphology of a wide variety of inorganic crystals. © 2014 American Institute of Chemical Engineers *AIChE J*, 60: 3707–3719, 2014

Keywords: crystal growth modeling, inorganic crystallization, periodic bond chain theory, spiral growth, bond valence model

Introduction

Crystal growth processes and crystal morphology govern the end-use functionality of inorganic solids in several application areas such as catalysis,[1] photovoltaics,[2] and so forth. Thus, it is important to have a mechanistic understanding of these processes to engineer the desired crystal shapes. For example, the {100} family of faces on Ag crystals exhibits higher selectivity toward ethylene epoxidation than the lower energy {111} faces.[3] Therefore, Ag nanocrystals with novel shapes have been synthesized that maximize the epoxidation selectivity.[4] Similarly, anatase (TiO_2) crystals normally grow in a tetragonal bipyramidal shape dominated by the {101} family of faces. However, the (001) face of anatase has a higher catalytic activity toward water dissociation than the (101) face.[5] The growth mechanism and the effect of growth environment parameters on the crystal morphology need to be well understood to grow silver crystals with {100} faces and anatase crystals with higher surface area of the (001) face.

The steady-state morphology achieved by a growing crystal depends on the growth kinetics of all the crystal faces.[6,7] When the surface integration of growth units is rate limiting, the crystal grows by the flow of steps across its surface. The growth units attach into special sites, knows as kink sites, along these steps. A kink site on the crystal surface is defined as the lattice position of a growth unit in which it is surrounded by exactly half of the solid-state neighbors as in the bulk crystal (also known as the half-crystal position).[8] The rate of crystal growth is fundamentally linked to the work done in adding a growth unit into the kink site.[9] Therefore, the solid-state interactions in the crystal must be studied in detail to create a mechanistic growth model for inorganic crystals.

Inorganic crystals are often composed of highly electropositive and electronegative atoms, so the solid-state intermolecular interactions are dominated by the electrostatic interactions. Normally, the long-range electrostatic interactions within ionic crystals are accounted for by using the Madelung constant, which is the ratio of the overall electrostatic interaction energy inside the bulk crystal relative to the nearest-neighbor electrostatic interaction energy.[10,11] However, this approach only captures the interactions in the bulk solid and does not consider the variation in the electronic structure at the growth surfaces. Our goal is to develop an engineering model suitable for product and process design that combines the concepts of bulk electrostatic interactions developed by Madelung[10] and Ewald[11] with the effect of the surface structure on the electronic properties of surface atoms of inorganic crystals. The partial charges of atoms in the bulk crystal differ from those on the surface and both differ from the classical valence charge or oxidation state. Quantum mechanical calculations and density functional theory can be used to calculate accurately the partial charges of bulk atoms as well as the surface atoms but it is impractical to perform these calculations on every face of every inorganic crystal. We find that for crystal growth models, the alternative approach provided by the bond valence

Additional Supporting Information may be found in the online version of this article.

Correspondence concerning this article should be addressed to M. F. Doherty at mfd@engineering.ucsb.edu.

model[12,13] delivers sufficiently accurate values of the partial charges of atoms on inorganic crystal surfaces without the need for electron density calculations.

In this work, we present a general method to identify the lattice directions along the strongest intermolecular interactions within inorganic crystals. Identifying these directions, also known as periodic bond chain (PBC) vectors,[14] is key to predicting the structure of the step edges and the shapes of growth spirals formed on crystal surfaces. The PBC directions on the cleavage plane of the calcite polymorph of calcium carbonate are identified, and the asymmetric shape of the growth spiral is attributed to the asymmetric structure of the step edges on the $(10\bar{1}4)$ calcite surface. The classical bond valence theory based on Pauling's rules for ionic bonding[15] is applied here to calculate the partial charges of surface ions as a function of their atomic surroundings. The potential energies of growth units situated in the kink sites along the edges of growth spirals can be calculated for inorganic crystals using a space partitioning method. This method, when applied to the kink sites on the $(10\bar{1}4)$ surface of calcite crystals, shows the quantitative basis for the asymmetry of the growth spirals and paves the way for a general mechanistic growth model to predict the crystal growth rates and morphologies of inorganic solids, including those with technological importance.

PBCs in Inorganic Crystals

Hartman and Perdok[14] proposed the concept of PBCs as the key link between the solid-state interactions and the kinetics of crystal growth. PBCs are chains of strong intermolecular interactions between growth units along a lattice direction which is called the PBC vector. These strong interactions are formed between the growth units (molecules/ions) during the crystallization process and therefore exclude any intragrowth-unit interactions. According to Hartman and Perdok,[14,16] PBCs must satisfy certain rules as listed below

1. A PBC must consist of uninterrupted chains of strong intermolecular interactions so that the crystal would grow in the direction of the PBC.

2. There must be a fundamental arrangement of growth units within the chain, also known as the structural period of the PBC, that is repeated by lattice translations along the PBC vector to obtain the entire PBC.

3. An intermolecular interaction between a pair of growth units cannot be shared by two PBCs in the same face of a crystal. An interaction may be shared between two PBCs that are not within the same crystal face.

4. The arrangement of growth units along a PBC direction must have the same stoichiometry as the overall stoichiometry of the crystal.

5. For nonpolar crystal structures (wherein the net dipole moment of the crystallographic unit cell is zero), the component of the electrostatic dipole moment perpendicular to the PBC vector must be zero.

The perpendicular dipole moment property is related to the stability of nonpolar crystal surfaces. Tasker proposed a stability criterion for ionic crystal surfaces based on the absence of a dipole moment perpendicular to the surface.[17] As a stable surface layer contains two or more PBCs, a net dipole moment perpendicular to the PBC vector results in a nonzero dipole moment perpendicular to the surface and will, therefore, destabilize the surface. Therefore, Tasker's criterion and the PBC property are self-consistent.

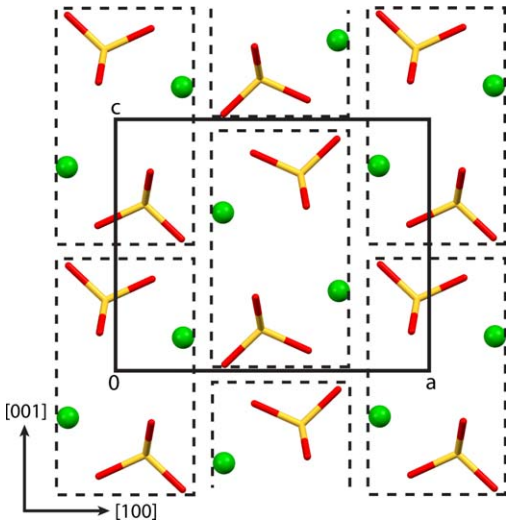

Figure 1. A view along the *b* axis of the barite ($BaSO_4$) unit cell.

The broken black rectangles show the building unit for PBCs in barite crystals. The solid black rectangle shows the edges of the unit cell. Barium atoms are represented by green spheres and sulfate growth unit by yellow (S) and red (O) capped sticks. Note that in this view, the fourth oxygen atom of the sulfate group overlaps with one of the other oxygen atoms and is therefore not visible. [Color figure can be viewed in the online issue, which is available at wileyonlinelibrary.com.]

If there is a polar axis present in the unit cell, all the PBCs in the crystal may have a net perpendicular dipole moment that is parallel to the polar axis direction. The surfaces of such crystals undergo reconstruction to stabilize the dipole moment perpendicular to the surface and the growth mechanisms of these polar surfaces are still debated.[18,19] However, we do not consider the growth of polar crystals in this article.

Building unit of the PBC

A systematic method to identify the PBCs in inorganic crystals must enforce the Hartman–Perdok rules discussed above, including the stoichiometry and perpendicular dipole moment properties. Inorganic crystals consist of ions as the growth units that are individually nonstoichiometric. Therefore, the PBCs must consist of stoichiometric groups of ions that are repeated throughout the crystal. We use the concept of a building unit of the PBC that has been used earlier for studying the PBCs in calcite ($CaCO_3$).[20,21] The building unit of a PBC is defined as a stoichiometric arrangement of ions such that its rotation and translation along the PBC vector direction will yield the entire bond chain. Thus, the dipole moment of the building unit must be zero if a single building unit has to yield all the PBCs in the crystal while satisfying the perpendicular dipole moment property for each individual PBC.

The building unit of a PBC must not be confused with the growth unit, the asymmetric unit, or the crystallographic unit cell. The growth unit is the solute species that is present in the growth environment (solution, vapor, etc.) and attaches into the kink sites on the crystal surface. A growth unit may be a molecule (e.g., for a paracetamol crystal), ion (e.g., for a calcium carbonate crystal), or a dimer (e.g., for an α-glycine crystal). Therefore, a growth unit may not always

be stoichiometric. A building unit is the fundamental unit of the PBCs in inorganic crystals and will typically consist of multiple growth units. Figure 1 shows the arrangement of Ba^{2+} and SO_4^{2-} growth units within the building unit, as well as in the crystallographic unit cell of barite ($BaSO_4$). The building unit for barite consists of two barium and two sulfate growth units and has zero dipole moment. The unit cell consists of four barium and four sulfate growth units while the asymmetric unit consists of one Ba, one S, and three O atoms.[22] We write the conventional notation for the ionic growth units with their oxidation states as superscripts with the understanding that these may not be the actual partial charges of these ions. The calculation of the actual partial charges on the ionic growth units will be discussed in the next section.

Once the building unit is identified based on the aforementioned properties, the symmetry operators of the unit cell are used to pack the crystal with building units. Uninterrupted chains joining these building units can be identified as the PBC directions. As the building unit is stoichiometric and has a zero dipole moment, the PBCs thus formed will satisfy the Hartman–Perdok rules.

Step edges from building units and PBCs

From a crystal growth perspective, the PBCs are important because the steps of a growth spiral or two-dimensional (2-D) nucleus on the crystal surface are parallel to the PBC vectors. Knowledge of all the PBC directions on any crystal surface will give the directions of the edges of a growth spiral and help predict its shape. The building unit and its arrangement along a PBC vector must eventually identify the structure of the step edges parallel to that PBC vector.

A step edge is the fundamental feature of a growth step on a crystal surface. Above absolute zero temperature, a straight step edge constantly rearranges under thermal fluctuations to a more favorable configuration such that there is always a finite density of kink sites along the step edge. A growth step moves by the incorporation of growth units into these kink sites present along the edge. Thus, the thickness of a step edge in the growth direction depends on the dimensions of the kink site which is usually 1 growth unit in thickness.

The arrangement of building units along the PBC direction may not give the exact step edge structure as the building unit usually consists of more than 1 growth unit. For example, Figure 2 shows that the arrangement of the building units along the [120] direction on the (210) surface of barite does not give the structure of the actual step edge that grows in the [001] direction. The arrangement of all the building units along a specific PBC direction must be decomposed into individual growth units and an arrangement of growth units along this specific PBC direction must be identified such that three conditions are satisfied—the resulting arrangement must (a) be stoichiometric, (b) have zero dipole moment perpendicular to the specific PBC vector, and (c) have dimensions ~1 growth unit thickness in the direction of the step motion. Figure 2 shows that the step edge structure along the [120] edge can be constructed from half of the contents of the arrangement of the building units along the [120] direction. A similar decomposition of the arrangement of the building units must be done for every PBC direction to correctly identify the structure of the step edge. In some cases, this decomposition can be more complicated

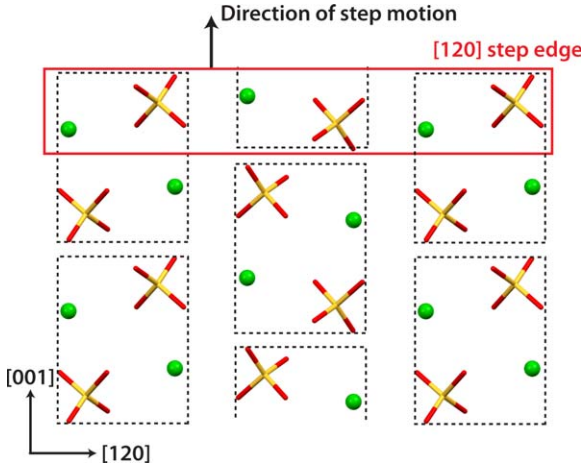

Figure 2. Crystal packing on the (210) barite surface.

The broken black rectangles form building units and the solid red rectangle shows the step edge along the [120] direction. The [120] step edge consists of half of the building unit arrangement while the other half forms part of another step edge parallel to the first one. [Color figure can be viewed in the online issue, which is available at wileyonlinelibrary.com.]

as the exact step edge structure may be formed out of chains of building units along two different PBC directions. This will be shown later in the article for the step edges on calcite surfaces.

Once the structure of the step edges along all the PBC directions is identified, the interaction energy along these edges is calculated to obtain the energy required to create kink sites from a straight step edge.[23] Electrostatic interactions dominate the lattice energy of inorganic crystals so the contribution of the long-range interactions in the PBC interaction energies must be calculated. For example, the ratio of the total interaction energy along the [100] PBC direction to the nearest-neighbor interaction energy for rock salt NaCl crystal is equal to $2\ln 2 = 1.386$.[24] The magnitude of the long-range (beyond nearest neighbor) interaction energy accounts for about 44% of the total interaction energy along the [100] PBC chain of rock salt NaCl crystals. Therefore, the energy calculations for inorganic crystals must never be limited to only nearest-neighbor interactions. The interaction energy for a growth unit along the PBC vector $\overrightarrow{v}$ direction is given by

$$E_{\mathrm{PBC},\overrightarrow{v}} = \frac{1}{2}\sum_{i=1}^{\infty}\left(\sum_{j=1}^{N_{\mathrm{GU}}} U_{i,j}\right) \tag{1}$$

$$U_{i,j} = \sum_{k=1}^{N_{\mathrm{GU},i}}\left(\frac{q_j q_k}{4\pi\epsilon_0 r_{jk}} + U_{j,k}^{\mathrm{sr}}\right) \tag{2}$$

where N_{GU} is the number of atoms in the central growth unit, $N_{\mathrm{GU},i}$ is the number of atoms in the growth unit i along the PBC vector $\overrightarrow{v}$. U^{sr} is the short-range interaction energy. A Buckingham potential is used to model the short-range interactions for most inorganic crystals.[25,26]

The framework developed here for identifying the building units, PBC directions, and step edge structures is completely general and can be applied to any inorganic crystal. The model requires the crystallographic unit cell data, the partial charges on the atoms of each growth unit in the bulk solid (obtained from quantum mechanical calculations), and a

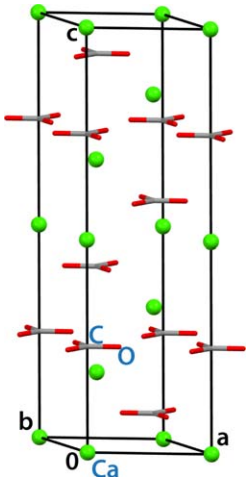

Figure 3. Calcite unit cell with the Ca atoms (green sphere) and CO_3 groups (gray and red capped sticks).

The contents of the asymmetric unit of the unit cell are labeled in blue. [Color figure can be viewed in the online issue, which is available at wileyonlinelibrary.com.]

suitable short-range intermolecular force field as inputs to identify the PBC directions in the crystal and calculate the interaction energy E_{PBC} along each PBC vector. We discuss the PBCs on calcite ($CaCO_3$) as an example in the following sections.

PBCs in bulk calcite

At ambient conditions, calcite is the most stable polymorph of crystalline calcium carbonate. It is ubiquitous in nature in the form of sedimentary and metamorphic rocks, cave formations, shells of marine organisms, and so forth. Crystal growth of calcite has been of special interest from a biomineralization perspective.[27] Pure calcite crystals occur in rhombohedral shape dominated by the $\{10\bar{1}4\}$ family of cleavage planes.[28] Calcite crystallizes in the $R\bar{3}c$ space group in the trigonal crystal system. The unit cell parameters for calcite are $a=b=4.988$ Å, $c=17.061$ Å, $\alpha=\beta=90^\circ$, $\gamma=120^\circ$.[29] Figure 3 shows the calcite unit cell with the arrangement of the Ca and CO_3 groups. The atoms within the asymmetric unit (which consists of one atom each of Ca, C, and O) are also labeled in Figure 3. The two orientations of the carbonate group in the calcite unit cell are related to each other by a 2_1 screw axis.

In trigonal and hexagonal lattice systems, the (hkl) Miller indices of a crystal face are often written in a four index notation as $(hkil)$, where $i=-h-k$. For example, the (104) crystal face of calcite is written as $(10\bar{1}4)$ in the four index notation. A lattice direction $[uvw]$ is written in the four index notation as $[\frac{2u-v}{3}\frac{2v-u}{3}\frac{-u-v}{3}w]$.[30] A lattice direction $[uvjw]$ can be written back in the three index notation as $[u-jv-jw]$. For example, the $[48\bar{1}]$ lattice direction in calcite crystal structure is written as $[\frac{8-8}{3}\frac{16-4}{3}\frac{-4-8}{3}\bar{1}]$ or $[04\bar{4}\bar{1}]$ in the four index notation. The $[04\bar{4}\bar{1}]$ direction can be converted back to the three index notation as the $[0-(-4)4-(-4)\bar{1}]$ or the $[48\bar{1}]$ direction. The four index notation is more popular for the Miller indices of crystal faces than for the lattice directions. We will use the four index notation to denote the crystal faces, and the three index notation to denote the lattice directions within calcite crystals.

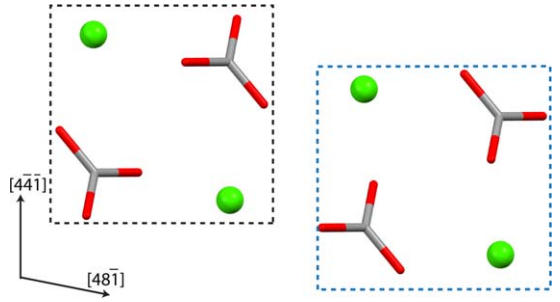

Figure 4. The two building units (enclosed within the broken black and blue rectangles) in calcite crystal and the arrangement of Ca^{2+} and CO_3^{2-} ions within each building unit.

The two building units are related to each other by a 2_1 screw axis. [Color figure can be viewed in the online issue, which is available at wileyonlinelibrary.com.]

The building unit of the PBCs in calcite crystals was identified using the properties discussed previously. Figure 4 shows the arrangement of Ca^{2+} and CO_3^{2-} ions within the building units. The two building units shown are related by a 2_1 screw axis and are, therefore, the same building unit with the composition $Ca_2C_2O_6$. Thus, a single building unit can be used to create all the PBCs in calcite using the symmetry operators present in the crystallographic unit cell. Figure 5 shows the packing of the entire unit cell with building units.

The packing of the building units on the $(10\bar{1}4)$ cleavage surface of calcite allows the identification of four PBC directions—$[\bar{4}41]$, $[48\bar{1}]$, $[42\bar{1}]$, and $[010]$. The structure of the step edges on the $\{10\bar{1}4\}$ calcite surface can be identified from the arrangement of the building units in each of these four PBC directions. The step edge in the $[48\bar{1}]$ direction contains only half of the contents of the building units, as shown in Figure 6. The same is true for the step edge structure in the $[\bar{4}41]$ direction.

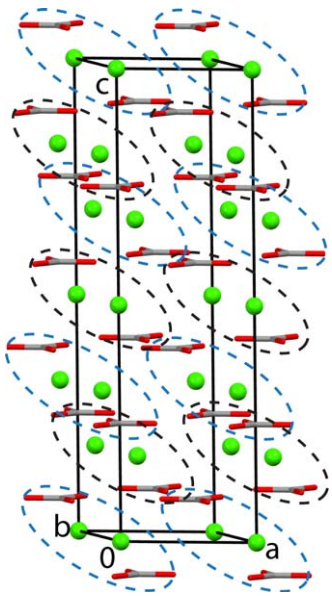

Figure 5. The packing of a calcite unit cell with building units (enclosed within broken blue and black ellipses).

[Color figure can be viewed in the online issue, which is available at wileyonlinelibrary.com.]

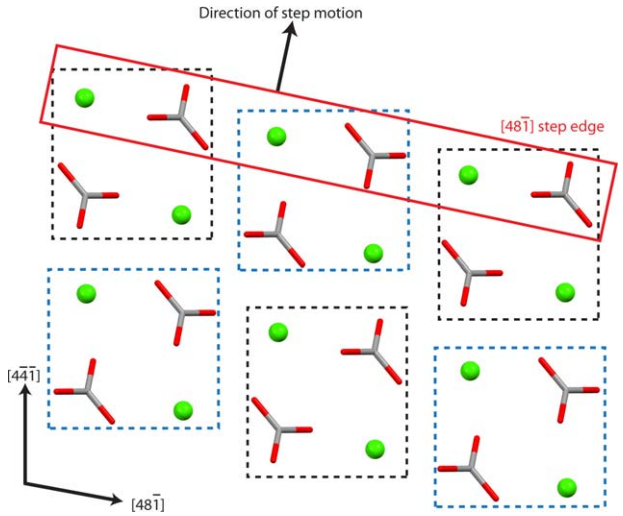

Figure 6. Crystal packing on the (10$\bar{1}$4) surface of calcite.

The broken black rectangles form building units and the solid red parallelogram shows the step edge along the [48$\bar{1}$] direction. The [48$\bar{1}$] step edge consists of half of the building unit contents while the other half forms part of another step edge parallel to the first one. [Color figure can be viewed in the online issue, which is available at wileyonlinelibrary.com.]

Figure 7 shows the step edge structures for the four PBCs on the (10$\bar{1}$4) surface of calcite. The step edges in both the [$\bar{4}$41] and [48$\bar{1}$] directions are stoichiometric and have zero dipole moment perpendicular to the edge direction. There are two sawtooth-shaped step edges, [010] and [42$\bar{1}$], that also possess these properties. However, the arrangement of growth units along the latter pair of PBCs are combinations of the chains in the [$\bar{4}$41] and [48$\bar{1}$] directions (as some of the interactions between the growth units along the [010] and [42$\bar{1}$] step edges are shared with the growth units along the [$\bar{4}$41] and [48$\bar{1}$] directions). Hence, there are only two independent PBCs on the (10$\bar{1}$4) surface of calcite. It is also evident that the structure of the PBCs in the [$\bar{4}$41] and [48$\bar{1}$] directions is identical. In fact, there are three families of symmetrically equivalent PBCs present in calcite crystal and they have been listed in Table 1. The average interaction energy (E_{PBC}) of a growth unit along each of these PBCs in the bulk crystal is also listed in Table 1. The interaction energies for the [010] and [42$\bar{1}$] families of PBCs are calculated fully counting the shared interactions with the [$\bar{4}$41] family of PBCs (i.e., as though the [$\bar{4}$41] family did not exist). The force field parameters including Buckingham potential parameters and partial charges were obtained from Raiteri et al.[31] A rigid model for the carbonate growth unit is used, which reproduces the bulk structural properties and the water interface equally well as compared to a flexible carbonate model.[32]

The lattice energy of calcite was calculated using the same force field parameters.[31] A Madelung sum was carried out for the electrostatic interactions, and the lattice energy remained constant with increasing supercell size beyond 60 × 60 × 20. A 10-Å cutoff was applied for the short-range interactions. The lattice energy was calculated as −671.7 kcal/mol for calcium carbonate, which matches very well with the reported value of −670.2 kcal/mol calculated from a Born–Fajans–Haber thermodynamic cycle.[33] The lattice energy of most inorganic crystals is an order of magnitude higher than that of most organic molecular crystals[34] and this difference is also manifested in the values of E_{PBC} for calcite.

There are four types of growth units in series along each of these edges—two Ca^{2+} and two CO_3^{2-} ions. The E_{PBC} values were calculated by averaging the interaction energies of all four growth units with all the other growth units along the semi-infinite chain parallel to the PBC vector direction. The E_{PBC} values in Table 1 show that the [$\bar{4}$41] family is the strongest family of PBCs in the calcite crystal. As discussed above, there are only two independent PBCs on the (10$\bar{1}$4) surface of calcite, therefore, the PBCs along the [$\bar{4}$41] and [48$\bar{1}$] directions will be the two PBCs present on this surface. This result is consistent with the earlier calculations of interaction energies of adjacent pairs of Ca^{2+} and CO_3^{2-} ions with the other ions in a semi-infinite chain along the PBC vector directions on the (10$\bar{1}$4) surface of calcite.[21] Because the [010] and [42$\bar{1}$] families of PBCs contain intermolecular interactions shared with the [$\bar{4}$41] and [48$\bar{1}$] PBCs, these two families of PBCs will not be considered further in this work. Figure 8 shows the shape of the growth spirals observed from atomic force microscopy (AFM) measurements on the (10$\bar{1}$4) surface of calcite.[35] The four-sided growth spiral is formed by the [$\bar{4}$41] and [48$\bar{1}$] step edges as predicted by the model.

From Figure 8, the growth spiral is asymmetric, such that the two opposite edges parallel to the [$\bar{4}$41] PBC vector grow at different step velocities.[36] The same is true for the step velocities of the two edges parallel to the [48$\bar{1}$] direction. However, the interaction energy values, E_{PBC}, reported in Table 1 are the same for both the opposite edges, denoted as [$\bar{4}$41]$_+$ and [$\bar{4}$41]$_-$. Therefore, the presence of asymmetric growth spirals on the (10$\bar{1}$4) surface of calcite cannot be explained on the basis of the PBC interaction energies in bulk calcite.

It has been postulated that the asymmetry of the growth spirals stems from the difference in the structure of the [$\bar{4}$41]$_+$ and [$\bar{4}$41]$_-$ edges.[37] As shown in Figure 9, the [$\bar{4}$41]$_+$ and [$\bar{4}$41]$_-$ edges form obtuse and acute angles,

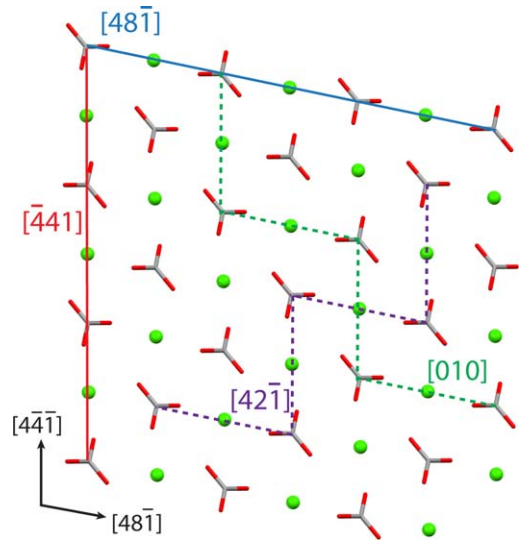

Figure 7. Step edges along various PBC directions on the (10$\bar{1}$4) surface of calcite.

The "straight" bond chains [$\bar{4}$41] and [48$\bar{1}$] are shown in solid red and blue lines, respectively. The "sawtooth" bond chains [010] and [42$\bar{1}$] are shown in broken green and broken purple lines, respectively. [Color figure can be viewed in the online issue, which is available at wileyonlinelibrary.com.]

Table 1. PBC Interaction Energies in Bulk Calcite Crystal

PBC Vector	E_{PBC} (kcal/mol of growth unit)
$[\bar{4}41]$, $[48\bar{1}]$, $[841]$	−140.7
[010], [100], [110]	−115.3
$[42\bar{1}]$, $[241]$, $[2\bar{2}1]$	−96.5

respectively, with the terrace plane. These edges are also referred to as the obtuse and acute edges, respectively.

Surface Effects on Solid-State Interactions

We hypothesize that the asymmetric structure of the opposite step edges on the $(10\bar{1}4)$ calcite surface and the resulting difference in the electronic properties of the atoms along these edges must result in a difference in the solid-state interactions between the growth units present along the $[\bar{4}41]_-$ acute and $[\bar{4}41]_+$ obtuse edges. This variation in the interaction energies will result in asymmetric step velocities for the acute and obtuse spiral edges on the $(10\bar{1}4)$ surface of calcite. A quantitative relationship between the environment of an atom and its partial charge is required to capture the difference in electronic properties of atoms between the obtuse and acute edges.

In the field of condensed matter physics, it is well known that the electronic structure (and hence the partial charge) of an atom is strongly related to the number and types of surrounding atoms and their distances from the central atom.[24] Knowledge of an atom's surroundings in the solid state has been one of the foundations of the ionic model of chemical bonding. Pauling proposed a set of five rules in 1929 that relate the crystal structure of an ionic solid to the properties of the constituent atoms.[15] These rules have been used to predict the crystal structure of ionic solids if the ionic radii and coordination numbers for the ions within the solid are known. One of the five rules relates the atomic charge on an anion, q_i, with the strength of the electrostatic bond S_{ij} that the anion i shares with its neighboring cation j in the solid[15]

$$q_i = -\sum_{j=1}^{CN_i}\left(\frac{q_j}{CN_j}\right) = -\sum_{j=1}^{CN_i} S_{ij} \tag{3}$$

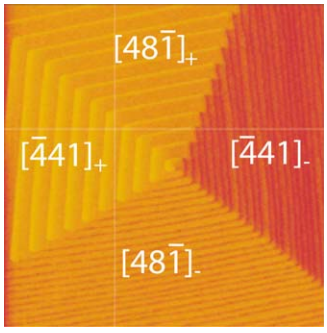

Figure 8. AFM image of a growth spiral on the $(10\bar{1}4)$ surface of calcite.

The image size is 3 × 3 μm. Adapted with permission from Davis et al., Am Mineral, 2004, 89, 714–720, © Mineralogical Society of America. [Color figure can be viewed in the online issue, which is available at wileyonlinelibrary.com.]

where CN_i and CN_j are the coordination numbers of the anion i and cation j, respectively. q_j is the charge on cation j and S_{ij} has units of electronic charge (Coulombs) and is always positive. The negative sign is introduced in Eq. 3 only to ensure that the charge q_i on anion i is always negative. For any ion in general, the charge is given by the summation of the bond strengths shared with its neighbors and the appropriate sign is affixed to the value of the summation depending on whether the ion is less or more electronegative than its neighbors (positive and negative signs, respectively).

Pauling's definition of the bond strength S can be used to calculate the partial charge of an ion only if the crystal structure has high symmetry such that all the bond strengths that a cation shares with its neighboring anions are equal (e.g., all nearest anionic neighbors are equidistant from the cation). This definition also does not account for the asymmetry in electrostatic bond strengths resulting from the relaxation of surface layers.

Bond valence model

A realistic quantification of the bond strength between atoms in inorganic crystals was made possible in the early 1970s when Donnay and Allmann proposed empirical relationships between the electrostatic bond strength s and the interionic distance.[38] Brown and Shannon[12] verified the generality of two Donnay and Allmann correlations between the bond strength s_{ij} and the interatomic distance r_{ij} between anion i and cation j

$$\left(\frac{s_{ij}}{e}\right) = \exp\left(\frac{R_0 - r_{ij}}{B}\right) \tag{4}$$

$$\left(\frac{s_{ij}}{e}\right) = \left(\frac{r_{ij}}{R_0}\right)^{-N} \tag{5}$$

where R_0, B, and N are parameters for each (i,j) pair and e is the elementary charge. R_0 and B have units of Å or nm and N is dimensionless. For crystals that contain polyatomic growth units (e.g., NH_4^+, CO_3^{2-}, etc.), each polyatomic ion is divided into individual atoms that possess net positive or negative charges. Thus, the crystal is treated as a collection

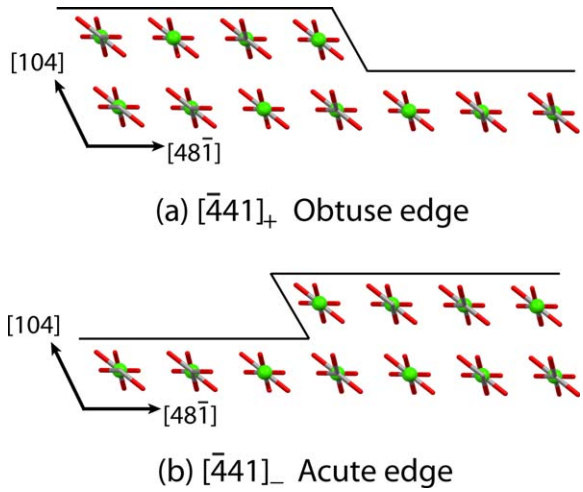

Figure 9. Side view of the $[\bar{4}41]$ edge on the $(10\bar{1}4)$ surface of calcite.

The $[\bar{4}41]_+$ and $[\bar{4}41]_-$ edges have been shown in (a) and (b), respectively, with the angle between the edge and the terrace being obtuse for the former and acute for the latter edge. [Color figure can be viewed in the online issue, which is available at wileyonlinelibrary.com.]

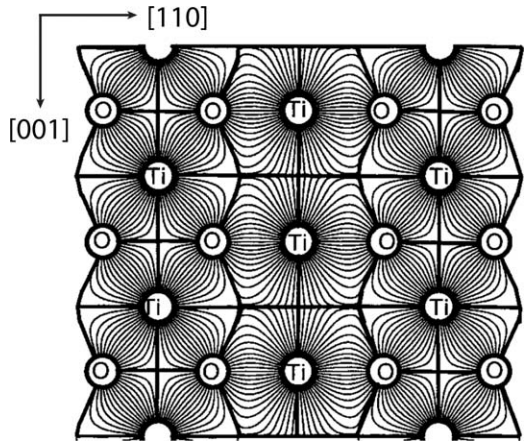

Figure 10. A representation of the electrostatic field in the (1$\bar{1}$0) face of rutile (TiO_2).

The light lines represent the electrostatic field lines and the thick lines show the zero-flux boundary that partitions space into bond regions. Adapted with permission from Preiser et al., Acta Crystallogr B, 1999, 55, 698–711, © International Union of Crystallography.

of individual charged atoms, not as a collection of monoatomic and polyatomic ions. For example, in calcite crystals, Eqs. 4 and 5 are written for two pairs of atoms, Ca—O and C—O. The Ca and C atoms in calcite are coordinated with 6 and 3 O atoms, respectively. Therefore, Eqs. 4 and 5 are written for each of the 6 Ca—O and 3 C—O pairs.

The empirical correlations shown in Eqs. 4 and 5 are robust such that the parameter values (R_0, B, and N) between a pair of atoms work well for any inorganic solid that contains this particular pair of atoms.[13] Although both the correlations work well, Eq. 4 is preferred because it reflects the repulsive potential between atoms and also because it is a well-behaved mathematical function at very small interatomic distances. To avoid confusion with Pauling's definition of bond strength, the quantity s_{ij} calculated from Eq. 4 is termed the bond valence between atoms i and j. This method is therefore called the bond valence model. Note that when all atomic neighbors in the coordination shell have the same charge and are all equidistant from the central ion, $s_{ij}=S_{ij}$.

The physical significance of the bond valence model and its applicability to quantify electrostatic interactions in inorganic solids has been studied in some detail.[39] The electrostatic field lines between two atoms in any inorganic solid are added up using Gauss' law to calculate the total electrostatic flux (normalized by the permittivity of free space ϵ_o) between the two atoms. For several inorganic crystals including calcite, aragonite, rutile, anatase, and so forth, the root mean squared error between the bond valences calculated from the interatomic distances (Eq. 4) and the total electrostatic flux calculated from Gauss' law was found to be less than $0.1e$.[39] This shows that the bond valence method accurately estimates the electrostatic interactions between two atoms in the solid state and, therefore, can be used to calculate the partial charges of atoms in inorganic crystals such as calcite. For example, the electrostatic field lines between the Ti and O atoms in the (1$\bar{1}$0) plane of rutile (TiO_2) crystals are shown in Figure 10.

The bond valence method assumes the fully ionic model for chemical bonding in inorganic crystals such that the partial charge of an atom obtained from the summation of its bond valences in the bulk is equal to its oxidation state. However, it is well known that most inorganic solids are not fully ionic. There is always some sharing of the electron density between the less electronegative and more electronegative atoms in the solid. Therefore, the actual atomic charge may not be equal to the oxidation state of the atom. Quantum mechanical calculations of bulk solids provide the accurate electron density distribution within the solid. Mulliken population analysis[40] and Bader charge partitioning[41] are two of the most widely used methods to partition the electron density between the atomic nuclei so that each atom can be assigned a partial charge. It is important to avoid the use of classical oxidation states on atoms in inorganic crystals as those charges overestimate the lattice energies.

The bond valence model can still be used to calculate the partial charges of surface atoms, provided the actual partial charges on the atoms in the bulk solid are known (e.g., from density functional theory calculations). The individual bond valences s_{ij} calculated from interatomic distances (e.g., from Eq. 4) must be scaled by the ratio of actual charge $q_{i,\text{actual}}$ to the oxidation state $q_{i,\text{OS}}$ of the atom i to give a normalized bond valence value s'_{ij} given by

$$s'_{ij}=s_{ij}\left(\frac{q_{i,\text{actual}}}{q_{i,\text{OS}}}\right) \tag{6}$$

where $q_{i,\text{OS}}=\sum_{j=1}^{\text{CN}_i} s_{ij}$ (i.e., Eq. 3) and $q_{i,\text{actual}}=\sum_{j=1}^{\text{CN}_i} s'_{ij}$. The normalized bond valence s'_{ij} should be used to calculate the actual partial charge $q_{i,\text{surf}}$ of atom i on the surface with coordination number $\text{CN}_{i,\text{surf}}$ as follows

$$q_{i,\text{surf}}=\sum_{j=1}^{\text{CN}_{i,\text{surf}}} s'_{ij} \tag{7}$$

Thus, the bond valence model can be used to calculate the actual partial charges on the surface atoms of any inorganic crystal if the interatomic distances between the surface atoms and their neighbors are known. Although this method may not be as accurate as quantum mechanical calculations on a crystal surface, it is much simpler and faster, and we have found it to be well suited to predicting crystal growth of inorganic solids such as calcite and aragonite.

Accurate information about the structure of both the surface and the growth medium close to the surface is required to calculate the surface charges using the bond valence model. Usually, surfaces of inorganic solids undergo relaxation and sometimes even reconstruct.[24] Experimental measurements of surface relaxation using diffraction-based methods such as low-energy electron diffraction can provide the positions of surface atoms and can be used to calculate the new distances between these atoms and their neighbors. Similarly, accurate information about the structure of solvent molecules around the surface atoms is needed to calculate the bond valence between the surface atoms and the solvent species. Experiments such as x-ray reflectivity measurements[42,43] and molecular simulations[31,44–46] can provide the distances between the surface or edge atoms and the solvent molecules. These inputs are required to accurately calculate the partial charges of atoms on inorganic crystal surfaces.

For bulk calcite crystal, the partial charges for atoms in the bulk were obtained from Raiteri et al.[31] They fitted the force field parameters including the partial charges against the measured structural and mechanical properties of calcite

Table 2. Bond Valence Parameters and Bond Valences for the Atom Pairs in Bulk Calcite

Atom Pair	R_0 (Å)	B (Å)	r_{ij} (Å)	s'_{ij} (e)
Ca and O	1.967	0.37	2.360	0.333
C and O	1.390	0.37	1.280	0.374

crystal, as well as, against the experimental free energy change (ΔG) of phase transition between calcite and aragonite. The reported values of the bulk partial charges for Ca, C, and O are +2, +1.123, and −1.041, respectively. The bond valence parameters for the two atom pairs (Ca—O and C—O) were obtained from a list of bond valence parameters hosted online by Brown.[47] Table 2 lists the bond valence parameters for the two pairs of atoms along with the interatomic distances in bulk calcite and bond valences scaled by their oxidation states. Calcite crystal structure has high symmetry such that each Ca atom is surrounded by six equidistant oxygen atoms and each C atom is surrounded by three equidistant oxygen atoms.

The bond valences for the O—H atom pair and their partial charges in liquid water were obtained from Brown[13] and the TIP3P model,[48] respectively, and are tabulated in Supporting Information Table S1. The distribution of water molecules around different surface species on calcite $(10\bar{1}4)$ surface was obtained from the molecular dynamics simulations performed by Wolthers et al.[44] They reported average distances between the water molecules near the surface and the calcite growth units in different surface positions (terrace/step/kink). The partial charges of Ca, C, and O atoms in different surface positions were calculated using these interatomic distances and the bond valence model. Table 3 lists the partial charges of Ca atoms in different lattice positions on the calcite $(10\bar{1}4)$ surface, and in the bulk. The partial charge on a Ca atom decreases as its location varies from inside the bulk solid to a kink site on a crystal surface. Although these charge values are calculated in the presence of water molecules, yet their presence does not fully compensate for the loss of solid-state coordination for surface species. The partial charge on the carbon atoms remains constant (+1.135) at every lattice position (bulk and surface) as it is always surrounded by its three neighboring oxygen atoms. The partial charges on the oxygen atoms in different lattice positions are tabulated in Supporting Information Table S2.

PBC energies on $(10\bar{1}4)$ surface of calcite

The interaction energies along the PBC directions on the $(10\bar{1}4)$ calcite surface will govern the density of kink sites along the spiral step edges and ultimately affect the growth kinetics of the spiral edges. The PBC interaction energies of growth units on calcite surface in contact with water are calculated from Eqs. 1 and 2 using the partial charges listed in Table 3 and Supporting Information Table S2. Because the partial charges of oxygen atoms on obtuse and acute edges are different, the interaction energies are calculated separately for both types of edges and reported in Table 4. There are four growth units (two Ca and two CO_3) along each of the four spiral edges on the $(10\bar{1}4)$ surface of calcite, and the interaction energy for each growth unit is reported along with the average interaction energy per growth unit for each edge.

For both the acute and obtuse edges in either $[\bar{4}41]$ or $[48\bar{1}]$ directions, the average interaction energy along the edge is exactly the same, similar to that in the bulk crystal. However, the individual interaction energies of the growth units differ between the acute and obtuse edges. Thus, different values of surface partial charges on the oxygen atoms of CO_3 groups on acute and obtuse edges (Supporting Information Table S2) result in the interaction energies being different on acute and obtuse edges for each of the four growth units. The value of E_{PBC} determines the work done to create kink sites from thermal rearrangement of a straight step edge,[49] therefore, we expect the density of kink sites to be different on obtuse and acute edges. The step velocity of a growing spiral edge depends on the density of kink sites along the edge[49] so this difference in E_{PBC} partially explains the asymmetric shape of growth spirals on the $(10\bar{1}4)$ surface of calcite. The step velocity also depends on the kinetics of incorporation into kink sites which is governed by the energetics of the kink site growth units, as discussed in the companion article.[50]

Kink Site Energies

The kinetics of crystal growth are governed by the energetics of the kink site position on the crystal surface.[8,51] The rate of attachment/detachment of growth units from the kink sites depends on the work done to attach/detach a growth unit from the kink site.[9] The work done in addition/removal of a growth unit to/from a kink site depends on the potential energy of the growth unit in the kink site, which is determined by the local structure of the crystalline solid as well as the growth medium. For organic crystals, the potential energies of growth units in the kink site positions on the crystal surface can be calculated by the addition of the nearest neighbor PBC interaction energies.[49] However, this method will not work for inorganic crystals as the electrostatic interactions contribute almost entirely to the lattice energy and there are strong interactions from non-nearest neighboring ions with like charge, which by definition cannot form PBCs. Therefore, such repulsive interactions are not accounted for when considering the PBC interaction energies and summing up only the PBC interaction energies will overestimate the magnitude of the potential energy of a kink site growth unit.

The potential energy of a growth unit in the kink site must be calculated by summing up all the atom–atom interactions over the entire three-dimensional (3-D) crystal. However, using a brute-force summation of the Coulombic interactions will be computationally prohibitive and will be repeated for every kink site along each edge on each crystal face. The Ewald summation method[11,52] has been applied to systems with uniform geometries and charges,[53,54] but it cannot be applied here as the partial charges on the atoms in the surface layer and along the step edge are different from the partial charges on atoms in the bulk. Therefore, we use the concept of space partitioning to calculate the kink site potential energies for inorganic crystals. The basic concept behind

Table 3. Partial Charges of Calcium Atoms in Calcite at Various Lattice Positions

Lattice Position	Partial Charge (e)
Bulk	+2.0
Terrace	+1.917
Edge (Acute or Obtuse)	+1.833
Kink	+1.750

Table 4. PBC Interaction Energies (E_{PBC}) in kcal/mol Along the Spiral Edges on the $(10\bar{1}4)$ Calcite Surface in Contact with Aqueous Solution

	Growth Unit				
Spiral Edge	Ca (1)	CO_3 (1)	Ca (2)	CO_3 (2)	Average
$[\bar{4}41]$ Obtuse	−104.9	−138.5	−104.9	−138.5	−121.7
$[\bar{4}41]$ Acute	−104.9	−139.6	−104.9	−137.4	−121.7
$[48\bar{1}]$ Obtuse	−104.9	−138.5	−104.9	−138.5	−121.7
$[48\bar{1}]$ Acute	−104.9	−139.6	−104.9	−137.4	−121.7

this method has been used successfully in the literature to calculate the surface Madelung constants for some inorganic crystals[55,56]

Space partitioning

Three-dimensional space can be partitioned into three types of components—axes, quadrants, and octants, which are one-, two-, and three-dimensional objects, respectively. Figure 11 shows the partitioning of the orthogonal coordinate system into these three types of objects. The 26 partitions in the 3-D orthogonal coordinate system and their mathematical notations have been listed in Supporting Information Table S3.

For a Kossel crystal with a growth unit at the center of the crystal and at the origin of the orthogonal coordinate system, the neighboring growth units in the solid state can be grouped into each of the 26 partitions of the 3-D space. The potential energy of the central growth unit can be divided into the additive contributions from growth units in each of those 26 partitions. This method assumes that the potential energy can be written as the sum of pairwise interaction energies alone and that the contribution of the three-body interactions is negligible.

Let us consider a kink site on the [100] edge of the (001) Kossel crystal surface (Figure 12). The growth unit in the kink site is at the origin of the coordinate system. By definition, the growth unit is in the half-crystal position[8] and is thus surrounded by exactly half of its solid-state neighbors in the bulk, that is, 13 partitions. The other 13 partitions of space form the growth medium and the interactions between the solvent species present in those partitions with the central growth unit will be calculated separately.

Table 5 lists the 13 partitions that form the solid-state neighbors of the growth unit in the kink site shown in Figure 12. Each of the growth units belonging to these 13 partitions contributes additively to the potential energy of the growth unit in the kink site. To calculate the energy contributions of each partition of space, it is necessary to classify each of the 13 partitions based on the effect of its location within the crystal on the partial charges of the atoms within the partition. The crystal surface or the terrace is assumed to be only a single atomic layer in thickness so that every layer below it is considered as bulk crystal. An octant can be either a part of the bulk crystal, or a part of the terrace and bulk crystal such that the top layer of the octant is part of the terrace and the rest behaves as bulk crystal. Similarly, a quadrant can be a part of bulk solid, bulk + terrace, only terrace, or terrace + step edge, depending on its location in the crystal. Finally, an axis could be part of the bulk solid, terrace, or edge. This classification makes it easier to quantify the electronic structure of atoms belonging to each part of the crystal. The partial charges of all the atoms in all possible crystal positions (bulk, terrace, step edge, kink, etc.) are calculated using the bond valence method. Table 5 lists the classification of the 13 solid-state partitions surrounding the kink site on the (001) Kossel crystal surface.

Once the atoms in each of the 13 solid-state partitions of space are grouped, the crystal packing in each of these partitions is generated and each atom within a partition is assigned the appropriate partial charge. The positions of the atoms in the surface layer and at edge positions are obtained from the amount of surface relaxation in presence of solvent that is obtained from either *in situ* diffraction experiments[57] or molecular simulations.[44] The interaction energies of all the atoms in the crystal with the atoms of the central growth unit can thus be calculated one partition at a time. The interaction energies from each partition of space, when they are part of the bulk crystal, can be calculated only once and stored to speed up calculations. These energy values can then be reused for any kink site depending on which

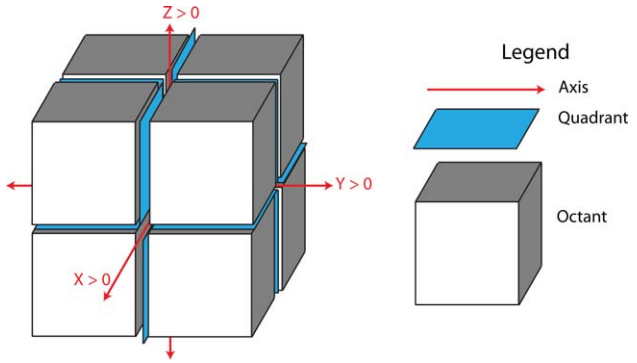

Figure 11. Partition of 3-D orthogonal space into octants (white and gray cubes), quadrants (blue squares), and axes (red lines).

[Color figure can be viewed in the online issue, which is available at wileyonlinelibrary.com.]

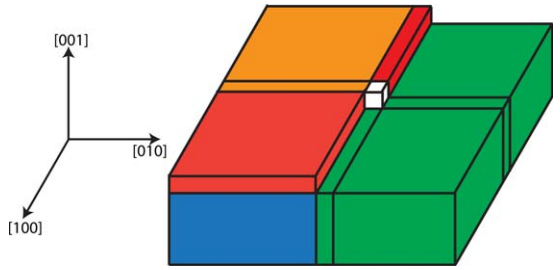

Figure 12. Classification of the 13 crystalline partitions around a kink site (white cube) on the [100] edge of the (001) Kossel crystal surface.

The partitions are colored corresponding to their classification listed in Table 5. [Color figure can be viewed in the online issue, which is available at wileyonlinelibrary.com.]

Table 5. Classification of the 13 Crystalline Partitions of Space Around a Kink Site Along the [100] Edge on the (001) Surface of a Kossel Crystal

	Notation			
Partition Type	X	Y	Z	Classification
Octant	<0	<0	<0	Bulk Solid
Octant	>0	<0	<0	
Quadrant	=0	<0	<0	
Quadrant	<0	=0	<0	
Axis	=0	=0	<0	
Octant	>0	>0	<0	Bulk + Surface
Octant	<0	>0	<0	
Quadrant	=0	>0	<0	
Quadrant	>0	=0	<0	
Quadrant	<0	<0	=0	Surface
Axis	=0	<0	=0	
Quadrant	>0	<0	=0	Surface+Edge Edge
Axis	<0	=0	=0	

partitions of space form part of the bulk crystal for that particular kink site. For crystallographic unit cells with a high degree of symmetry, many of these partitions of space will be symmetrically equivalent and will contribute equally to the kink site potential energy. This symmetry equivalence should be exploited to further save computational efforts.

This analysis works with minor modifications for a non-orthogonal crystal structure. The lattice spacing or the interaction energies along the three cardinal directions need not be symmetric. This method can be applied to any crystal structure once the three strongest PBC directions are identified. Placing the three cardinal directions (X, Y, Z in the Kossel crystal example) along the three strongest PBC directions of the crystal will simplify the kink site energy calculations as the step edges of growth spirals will be aligned with these cardinal directions. The classification of the 13 partitions of space that form the crystal will thus be straightforward.

If two PBCs that are present in two different F-faces share an intermolecular interaction, the choice of the cardinal directions may not be unique for the entire crystal. For example, if the PBCs in X and Z directions share a common bond, then the space partitioning for the face containing X and Y PBCs cannot be carried out with Z as the third cardinal direction. If X and Z were both chosen as the cardinal directions, the growth units between which the shared interaction exists, will simultaneously belong to two different space partitions. Therefore, the three cardinal directions are chosen separately for each F-face to ensure that only one of the PBCs with the shared interaction is a part of the space partitioning analysis. For example, some PBCs in aragonite ($CaCO_3$) crystals share intermolecular interactions, and the space partitioning in aragonite crystals will be discussed elsewhere (Dandekar and Doherty, in preparation).

The interactions between the species of the growth medium and the kink site growth unit cannot be calculated using this space partitioning method. As the growth medium or solvent does not have a periodic structure, it is impossible to calculate the long-range electrostatic interaction energies between kink site growth unit and the solvent molecules without performing a molecular dynamics simulation to determine the solvent structure around the kink site. If the solvent molecules near the crystal surface are assumed to screen the kink site growth unit, the interaction energy with solvent molecules can be calculated once their distribution near the kink site is known.[44]

Kink site energies on $(10\bar{1}4)$ surface of calcite

We chose the three PBC directions in the $[\bar{4}41]$ family with the strongest PBC interaction energy in bulk calcite (Table 1) as the three cardinal directions to apply the space partitioning method to calculate kink site energies on calcite crystal surfaces. Table 6 shows the kink site potential energies, U_{kink}, for all the kink sites on the spiral edges of the $(10\bar{1}4)$ face of calcite. There are two edge directions $[\bar{4}41]$ and $[48\bar{1}]$ on the $(10\bar{1}4)$ surface and each edge has an obtuse and acute orientation, resulting in a total of four spiral edges. Each edge has four types of growth units (two Ca and two CO_3). There are two orientations ($\mathscr{E}$ and $\mathscr{W}$) for each kink site on a spiral edge. Therefore, there are a total of $4\times4\times2 = 32$ types of kink sites on the $(10\bar{1}4)$ surface of calcite. When the edge grows in the North direction (Figure 13), a kink site in the $\mathscr{E}$ orientation faces the East direction, whereas the kink site in the $\mathscr{W}$ orientation faces the West direction.

The symmetry equivalence between the kink sites on the $[\bar{4}41]$ and $[48\bar{1}]$ edges is apparent from the kink site potential energies reported in Table 6. The potential energy of the Ca (1) kink site ($\mathscr{E}$ orientation) on the $[\bar{4}41]$ obtuse edge is exactly equal to that of the Ca (2) kink site ($\mathscr{W}$ orientation) on the $[48\bar{1}]$ obtuse edge and so on. The kink site potential energies U_{kink} calculated for the obtuse and acute edges of the growth spirals on calcite $(10\bar{1}4)$ surface are not equal to each other as shown in Table 6. As the attachment/detachment rate from the kink sites and the step velocity depends on the kink site potential energy,[49,58] the U_{kink} values suggest that the step velocities of obtuse and acute edges should be different. Therefore, the difference in the solid-state interaction energies in the kink sites between acute and obtuse spiral edges provides a quantitative explanation for the presence of asymmetric growth spirals on the $(10\bar{1}4)$ surface of calcite.

Discussion

There is a significant body of literature to identify the PBCs in inorganic solids. Hartman wrote several articles that identify PBCs in inorganic crystals such as barite,[16,59]

Table 6. Kink Site Potential Energy (U_{kink}) in kcal/mol for the 32 Kink Sites on the $(10\bar{1}4)$ Surface of Calcite

		U_{kink}	(kcal/mol)
Edge Type	Growth Unit	$\mathscr{E}$	$\mathscr{W}$
$[\bar{4}41]$ Obtuse	Ca (1)	−316.8	−311.3
	CO_3 (1)	−332.2	−344.5
	Ca (2)	−318.0	−312.6
	CO_3 (2)	−333.7	−345.9
$[\bar{4}41]$ Acute	Ca (1)	−307.7	−305.6
	CO_3 (1)	−345.8	−346.5
	Ca (2)	−312.6	−314.7
	CO_3 (2)	−344.6	−345.2
$[48\bar{1}]$ Obtuse	Ca (1)	−312.6	−318.0
	CO_3 (1)	−345.9	−333.7
	Ca (2)	−311.3	−316.8
	CO_3 (2)	−344.5	−332.2
$[48\bar{1}]$ Acute	Ca (1)	−314.7	−312.6
	CO_3 (1)	−345.2	−344.6
	Ca (2)	−305.6	−307.7
	CO_3 (2)	−346.5	−345.8

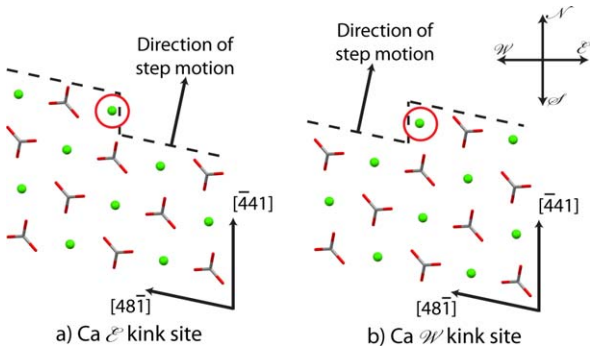

Figure 13. A plan view of the $(10\bar{1}4)$ surface of calcite showing the two orientations (a) $\mathscr{E}$ and (b) $\mathscr{W}$ of Ca kink sites on the $[48\bar{1}]$ obtuse edge.

The kink site Ca atoms are enclosed within the red circles. [Color figure can be viewed in the online issue, which is available at wileyonlinelibrary.com.]

sphalerite,[60] cadmium iodide,[61] tin iodide,[62] rutile,[63] cotunnite,[64] corundum,[65] yttrium barium copper oxide,[66] gypsum,[67] and so forth. A graph theoretic method was developed by Strom[68,69] to identify the PBCs in ionic solids based on the Hartman–Perdok rules. We have developed another systematic method that can help identify the PBC structures within any inorganic solid, and can be applied within the framework of a mechanistic crystal growth model.

The original definition of the building unit of a PBC was based on a stoichiometric arrangement of neighboring growth units.[21,70] For example, in an AB type crystal, each A-B neighboring pair in the solid state was identified as the building unit for the PBC direction parallel to the lattice vector joining the A-B pair. Thus, the structure of a building unit was uniquely defined for every PBC direction and the identification of one building unit did not provide any information about either the structure of the other building units, or the directions of other PBC vectors. We impose an additional condition on the structure of the building unit, that its dipole moment must be zero. This condition results in a building unit structure that is identical for all the PBCs, and therefore, for the entire crystal. Thus, the identification of the PBC vectors in an inorganic solid is reduced to the identification of a single building unit and then applying the symmetry operators in the unit cell to obtain the crystal packing with building units. The arrangement of building units along a PBC direction may not be equal to the actual structure of the step edge. Therefore, the arrangement of building units along each PBC vector must be decomposed into an arrangement of growth units that follows Hartman–Perdok rules. The identification of PBCs in inorganic solids can now be carried out in a systematic step-by-step methodology, which is discussed in Supporting Information in detail.

A more important aspect of our model is the practical implementation of quantum mechanical concepts that govern the electronic properties of the growth units situated on crystal surfaces. The importance of partial charges of surface atoms on thermodynamics and kinetics of crystal growth has been known for some time. Polar morphologies of sodium chlorate[71] and sodium periodate[72] have been explained, using the attachment energy model, on the basis of different partial charges (calculated using quantum mechanics) on the opposite crystal faces. Knowledge of the partial charges in bulk solid combined with the bond valence model allows the calculation of partial charges in surface positions with different solid-state coordination. The effect of the solvent molecules next to the crystal surface on the partial charges of surface atoms is also captured within the bond valence framework. A space partitioning method allows easy calculation of kink site potential energies while accounting for the different values of surface charges and all the long-range interactions. This model provides a useful engineering solution to the problem of identification of PBC directions on inorganic crystal surfaces and the calculation of interaction energies on the surface that govern the kinetics of layered growth on these crystal surfaces.

Crystal growth on zeolite surfaces has been studied extensively to attain desirable crystal shapes for various zeolite systems such as ZSM-5,[73] silicalite-1,[74] zeolite L,[75,76] and so forth. We expect that our model is capable of predicting the shapes of growth spirals[77,78] and 2-D nuclei[79,80] observed experimentally on zeolite surfaces. We further expect this method, that calculates long-range electrostatic interaction energies on inorganic crystal surfaces, can be applied with a mechanistic growth model[50] to design functionally desirable zeolite crystals.

Conclusions

In this article, we have discussed a generalized model capable of capturing the solid-state interactions in inorganic crystals from a crystal growth perspective. This approach is based on identifying the directions of strongest intermolecular interactions within the crystal while accounting for long-range electrostatic interactions and stoichiometry. The model can help predict the shape of growth spirals formed on inorganic crystal surfaces such as the calcite $(10\bar{1}4)$ surface.

The growth kinetics of inorganic crystals depends on the Coulombic interactions of the growth units in the kink site positions on crystal surfaces. The change in the electronic structure of surface atoms from those in the bulk has been captured using the bond valence model and a systematic method is presented to calculate the partial charges of atoms located in different lattice positions on inorganic crystal surfaces. The concept of space partitioning was used to partition a growing crystal into parts that belong to the bulk crystal or terrace or step edge. This classification simplifies the calculation of the potential energies of growth units in the kink site positions on an inorganic crystal surface. The potential energy calculations for kink sites on the $(10\bar{1}4)$ calcite surface explain the asymmetric growth of the obtuse and acute edges. This framework lays the foundation for a mechanistic crystal growth model that is capable of predicting the shapes of solution grown inorganic crystals such as calcite, titanium dioxide, barite, and so forth, which will be discussed in another article.

Acknowledgment

The authors are grateful for the financial support provided by the U.S. Army Research Office through the Institute of Collaborative Biotechnologies at the University of California, Santa Barbara (contract no. W911NF-09-D-0001), the Dow Chemical Company for endowing a doctoral fellowship

awarded to P.D., and by the National Science Foundation through CBET-1159746 (M.F.D.).

Literature Cited

1. Zhang J, Ohara S, Umetsu M, Naka T, Hatakeyama Y, Adschiri T. Colloidal ceria nanocrystals: a tailor-made crystal morphology in supercritical water. *Adv Mater*. 2007;19:203–206.
2. Yuhas BD, Yang P. Nanowire-based all-oxide solar cells. *J Am Chem Soc*. 2009;131:3756–3761.
3. Christopher P, Linic S. Shape- and size-specific chemistry of Ag nanostructures in catalytic ethylene epoxidation. *ChemCatChem*. 2010;2:78–83.
4. Linic S, Christopher P. Overcoming limitation in the design of selective solid catalysts by manipulating shape and size of catalytic particles: epoxidation reactions on silver. *ChemCatChem*. 2010;2:1061–1063.
5. Yang HG, Sun CH, Qiao SZ, Zou J, Liu G, Smith SC, Cheng HM, Lu GQ. Anatase TiO_2 single crystals with a large percentage of reactive facets. *Nature*. 2008;453:638–641.
6. Frank FC. On the Kinematic Theory of Crystal Growth and Dissolution Processes. *Growth and Perfection of Crystals*. New York: Wiley, 1958:411–419.
7. Chernov AA. The kinetics of the growth forms of crystals. *Sov Phys Crystallogr*. 1963;7:728–730.
8. Stranski IN. Zur theorie des kristallwachstums. *Z Phys Chem*. 1928; 136:259–278.
9. Markov IV. *Crystal Growth for Beginners, Fundamentals of Nucleation, Crystal Growth and Epitaxy*. Singapore: World Scientific, 2003.
10. Madelung E. Das elektrische Feld in Systemen von regelmassig angeordneten Punktladungen. *Phys Zs*. 1918;19:524–533.
11. Ewald PP. Die Berechnung optischer und elektrostatischer Gitterpotentiale. *Ann Phys*. 1921;64:253–287.
12. Brown ID, Shannon RD. Empirical bond-strength-bond-length curves for oxides. *Acta Crystallogr A*. 1973;29:266–282.
13. Brown ID. *The Chemical Bond in Inorganic Chemsitry: The Bond Valence Model*. New York, NY: Oxford University Press, 2002.
14. Hartman P, Perdok WG. On the relations between structure and morphology of crystals. I. *Acta Crystallogr*. 1955;8:49–52.
15. Pauling L. The principles determining the structure of complex ionic crystals. *J Am Chem Soc*. 1929;51:1010–1026.
16. Hartman P, Perdok WG. On the relations between structure and morphology of crystals. III. *Acta Crystallogr*. 1955;8:525–529.
17. Tasker PW. The stability of ionic crystal surfaces. *J Phys C Solid State*. 1979;12:4977–4984.
18. Noguera C. Polar oxide surfaces. *J Phys: Condens Matter*. 2000;12: R367.
19. Diebold U, Li SC, Schmid M. Oxide surface science. *Annu Rev Phys Chem*. 2010;61:129–148.
20. Heijnen WMM. The morphology of gel grown calcite. *N Jb Miner Mh*. 1985;8:357–371.
21. Aquilano D, Calleri M, Natoli E, Rubbo M, Sgualdino G. The {1 0 4} cleavage rhombohedron of calcite: theoretical equilibrium properties. *Mater Chem Phys*. 2000;66:159–163.
22. Miyaka M, Minato I, Morikawa H, Iwai S. Crystal structures and sulphate force constants of barite, celestite and anglesite. *Am Mineral*. 1978;63:506–510.
23. Burton WK, Cabrera N, Frank FC. The growth of crystals and the equilibrium structure of their surfaces. *Philos Trans R Soc A*. 1951; 243:299–358.
24. Kittel C. *Introduction to Solid State Physics*. Hoboken, NJ: Wiley, 2005.
25. Catlow CRA, Dixon M, Mackrodt WC. Interionic potentials in ionic solids. *Computer Simulation of Solids*. Berlin: Springer-Verlag, 1982:130–161.
26. Gale JD, Rohl AL. The general utility lattice program (GULP). *Mol Simul*. 2003;29:291–341.
27. Morse JW, Arvidson RS, Lüttge A. Calcium carbonate formation and dissolution. *Chem Rev*. 2007;107:342–381.
28. Alkivar. Large crystal of Icelandic Spar (Calcite) on display at the National Museum of Natural History Washington, DC. 2005. Available at https://upload.wikimedia.org/wikipedia/commons/3/37/Calcite-HUGE.jpg. Accessed on November 21, 2005.
29. Markgraf S, Reeder R. High-temperature structure refinements of calcite and magnesite. *Am Mineral*. 1985;70:590–600.
30. Giacovazzo C, Monaco HL, Viterbo D, Scordari F, Gilli G, Zanotti G, Catti M. *Fundamentals of Crystallography*. New York: Oxford University Press, 1992.
31. Raiteri P, Gale JD, Quigley D, Rodger PM. Derivation of an accurate force-field for simulating the growth of calcium carbonate from aqueous solution: a new model for the calcite-water interface. *J Phys Chem C*. 2010;114:5997–6010.
32. Raiteri P, Gale JD. Water is the key to nonclassical nucleation of amorphous calcium carbonate. *J Am Chem Soc*. 2010;132:17623–17634.
33. Jenkins HDB, Pratt KF, Smith BT. Lattice potential energies for calcite, aragonite and vaterite. *J Inorg Nucl Chem*. 1976;38:371–377.
34. Winn D, Doherty MF. Modeling crystal shapes of organic materials grown from solution. *AIChE J*. 2000;46:1348–1367.
35. Davis KJ, Dove PM, Wasylenki LE, De Yoreo JJ. Morphological consequences of differential Mg^{2+} incorporation at structurally distinct steps on calcite. *Am Mineral*. 2004;89:714–720.
36. Teng HH, Dove PM, Orme CA, De Yoreo JJ. Thermodynamics of calcite growth: Baseline for understanding biomineral formation. *Science*. 1998;282:724–727.
37. Paquette J, Reeder RJ. Relationship between surface structure, growth mechanism, and trace element incorporation in calcite. *Geochim Cosmochim Acta*. 1995;59:735–749.
38. Donnay G, Allmann R. How to recognize O^{2-}, OH^-, and H_2O in crystal structures determined by X-rays. *Am Mineral*. 1970;55:1003–1015.
39. Preiser C, Lösel J, Brown ID, Kunz M, Skowron A. Long-range Coulomb forces and localized bonds. *Acta Crystallogr B*. 1999;55: 698–711.
40. Mulliken RS. Electronic population analysis on LCAO[Single Bond]MO Molecular Wave Functions. I. *J Chem Phys*. 1955;23: 1833–1840.
41. Tang W, Sanville E, Henkelman G. A grid-based Bader analysis algorithm without lattice bias. *J Phys: Condens Matter*. 2009;21: 084204.
42. Fenter P, Sturchio N. Calcite (104)-water interface structure, revisited. *Geochim Cosmochim Acta*. 2012;97:58–69.
43. Fenter P, Kerisit S, Raiteri P, Gale JD. Is the calcite-water interface understood? direct comparisons of molecular dynamics simulations with specular X-ray reflectivity data. *J Phys Chem C*. 2013;117:5028–5042.
44. Wolthers M, Di Tommaso D, Du Z, de Leeuw NH. Calcite surface structure and reactivity: molecular dynamics simulations and macroscopic surface modelling of the calcite-water interface. *Phys Chem Chem Phys*. 2012;14:15145–15157.
45. Stack AG, Raiteri P, Gale JD. Accurate rates of the complex mechanisms for growth and dissolution of minerals using a combination of rare-event theories. *J Am Chem Soc*. 2012;134:11–14.
46. Raju M, Kim SY, van Duin ACT, Fichthorn KA. ReaxFF reactive force field study of the dissociation of water on titania surfaces. *J Phys Chem C*. 2013;117:10558–10572.
47. Brown ID. *Accumulated Table of Bond Valence Parameters*. 2006.
48. Jorgensen WL, Chandrasekhar J, Madura JD, Impey RW, Klein ML. Comparison of simple potential functions for simulating liquid water. *J Chem Phys*. 1983;79:926–935.
49. Kuvadia ZB, Doherty MF. Spiral growth model for faceted crystals of non-centrosymmetric organic molecules grown from solution. *Cryst Growth Des*. 2011;11:2780–2802.
50. Dandekar P, Doherty MF. A mechanistic growth model for inorganic crystals: growth mechanism. *AIChE J*. In press.
51. Kossel W. Zur Theorie des Kristallwachstums. *Nachur Ges Wiss Göttingen*. 1927;206:135–143.
52. Darden T, York D, Pedersen L. Particle mesh Ewald: an $N.log(N)$ method for Ewald sums in large systems. *J Chem Phys*. 1993;98: 10089–10092.
53. Parry D. The electrostatic potential in the surface region of an ionic crystal. *Surf Sci*. 1975;49:433–440.
54. Yeh IC, Berkowitz ML. Ewald summation for systems with slab geometry. *J Chem Phys*. 1999;111:3155–3162.
55. Levine JD, Mark P. Theory and observation of intrinsic surface states on ionic crystals. *Phys Rev*. 1966;144:751–763.
56. Garrone E, Zecchina A, Stone FS. An experimental and theoretical evaluation of surface states in MgO and other alkaline earth oxides. *Philos Mag B*. 1980;42:683–703.
57. Heberling F, Trainor TP, Lützenkirchen J, Eng P, Denecke MA, Bosbach D. Structure and reactivity of the calcite-water interface. *J Colloid Interface Sci*. 2011;354:843–857.

58. Kim SH, Dandekar P, Lovette MA, Doherty MF. Kink rate model for the general case of organic molecular crystals. *Cryst Growth Des*. 2014;14:2460–2467.
59. Hartman P, Strom C. Structural morphology of crystals with the barite ($BaSO_4$) structure: a revision and extension. *J Cryst Growth*. 1989;97:502–512.
60. Hartman P. An approximate calculation of attachment energies for ionic crystals. *Acta Crystallogr*. 1956;9:569–572.
61. Hartman P. The Madelung constants of slices and chains, with an application to the CdI_2 structure. *Acta Crystallogr*. 1958;11:365–369.
62. Hartman P. Theoretical morphology of crystals with the SnI4 structure. *J Cryst Growth*. 1968;2:385–394.
63. Hartman P. *Crystal Growth: An Introduction. North-Holland Series in Crystal Growth*. Amsterdam: North-Holland Publishing Co, 1973.
64. Woensdregt C, Hartman P. Structural morphology of cotunnite, PbCl2, laurionite, Pb(OH)Cl, and SbSI. *J Cryst Growth*. 1988;87: 561–566.
65. Hartman P. The effect of surface relaxation on crystal habit: cases of corundum (α-Al_2O_3) and Hematite (α-Fe_2O_3). *J Cryst Growth*. 1989; 96:667–672.
66. Sun B, Hartman P, Woensdregt C, Schmid H. Structural morphology of $YBa_2Cu_3O_{7-x}$. *J Cryst Growth*. 1990;100:605–614.
67. Heijnen W, Hartman P. Structural morphology of gypsum ($CaSO_4.2H_2O$), brushite ($CaHPO_4.2H_2O$) and pharmacolite ($CaHAsO_4.2H_2O$). *J Cryst Growth*. 1991;108:290–300.
68. Strom CS. Graph-theoretic construction of periodic bond chains. *Z Kristallogr*. 1980;153:99–113.
69. Strom CS. Graph-theoretic construction of periodic bond chains II. Ionic case. *Z Kristallogr*. 1981;154:31–43.
70. Abbona F, Aquilano D. Morphology of crystals grown from solutions. *Springer Handbook of Crystal Growth*. Berlin Heidelberg: Springer-Verlag, 2010:53–92.
71. Clydesdale G, Roberts KJ, Telfer GB, Saunders VR, Pugh D, Jackson RA, Meenan P. Prediction of the polar morphology of sodium chlorate using a surface-specific attachment energy model. *J Phys Chem B*. 1998;102:7044–7049.
72. Soltzberg LJ, Madden E. Crystal morphology prediction and morphology variation in $NaIO_4$ and $NaIO_4.3H_2O$. *Acta Crystallogr*. 1999;B55:882–885.
73. Bonilla G, Diaz I, Tsapatsis M, Jeong HK, Lee Y, Vlachos DG. Zeolite (MFI) crystal morphology control using organic structure-directing agents. *Chem Mater*. 2004;16:5697–5705.
74. Davis TM, Drews TO, Ramanan H, He C, Dong J, Schnablegger H, Katsoulakis MA, Kokkoli E, McCormick AV, Penn RL, Tsapatsis M. Mechanistic principles of nanoparticle evolution to zeolite crystals. *Nat Mater*. 2006;5:400–408.
75. Brent R, Lobo AJW, Lewis DW, Anderson MW. Modifying the crystal habit of zeolite L by addition of an organic space filler. *J Phys Chem C*. 2010;114:18240–18246.
76. Lupulescu AI, Kumar M, Rimer JD. A facile strategy to design zeolite L crystals with tunable morphology and surface architecture. *J Am Chem Soc*. 2013;135:6608–6617.
77. Dumrul S, Bazzana S, Warzywoda J, Biederman RR, Sacco A Jr. Imaging of crystal growth-induced fine surface features in zeolite A by atomic force microscopy. *Microporous Mesoporous Mater*. 2002; 54:79–88.
78. Cubillas P, Anderson MW, Attfield MP. Crystal growth mechanisms and morphological control of the prototypical metal-organic framework MOF-5 revealed by atomic force microscopy. *Chem Eur J*. 2012;18:15406–15415.
79. Cubillas P, Stevens SM, Blake N, Umemura A, Chong CB, Terasaki O, Anderson MW. AFM and HRSEM invesitigation of zeolite A crystal growth. Part 1: in the absence of organic additives. *J Phys Chem C*. 2011;115:12567–12574.
80. Holden MA, Cubillas P, Attfield MP, Gebbie JT, Anderson MW. Growth mechanism of microporous zincophosphate sodalite revealed by in situ atomic force microscopy. *J Am Chem Soc*. 2012;134: 13066–13073.

Manuscript received Mar. 14, 2014 .